Geometry and Heat Loss in Channel Flow of a Fluid with Temperature-Dependent Density

Stephen E. Bechtel, Dongbu Cao, and Hsien-fu Hsiao
Dept. of Aerospace Engineering, Applied Mechanics, and Aviation,
The Ohio State University, Columbus, OH 43210

Cao et al. previously derived a thermomechanically constrained theory for materials with temperature-dependent density and applied it to the illustrative problem of plane Poiseuille flow between isothermal walls. Here the theory is applied to geometries and thermal boundary conditions of practical importance in polymer processing: flows through planar, circular and annular dies with heat loss through the die walls. How geometry and thermal boundary conditions combine with material properties, especially thermal expansivity, to effect velocity and temperature profiles, and mass and volume flow rates is explored. A comparison is made with predictions that follow if temperature-dependence of density is either ignored or handled (as is the standard practice) by a posteriori insertion of a temperature-dependent expression for density into equations derived for constant density.

Introduction

In general, material properties depend on both thermal and mechanical state variables. In many polymer processes the mechanical dependence of density, specific heat, viscosity, and thermal conductivity is weak, due to the low to moderate pressure levels encountered in these processes (Cox and Macosko, 1974; Lodge and Ko, 1989; Spencer and Gilmore, 1950; Winter, 1977), and can be neglected. In contrast, temperatures are high enough and the temperature changes and gradients are sufficiently large that the temperature dependence of material properties must be incorporated. Temperature dependence of specific heat c, viscosity μ, and thermal conductivity k can be straightforwardly modeled by inserting temperature-dependent expressions $c(\theta)$, $\mu(\theta)$, $k(\theta)$ (where θ denotes absolute temperature) into the momentum and energy equations for an incompressible material, but not density. This is because specifying density as a function $\rho(\theta)$ of temperature is fundamentally inconsistent with the constraint of incompressibility on which these equations are based. The temperature dependence of density demands the thermomechanical constraint

$$\operatorname{div} \boldsymbol{v} = -\frac{\rho'(\theta)}{\rho(\theta)}\dot{\theta}, \tag{1}$$

where $\boldsymbol{v}$ is the velocity and $\rho'(\theta)$ denotes the derivative of $\rho(\theta)$ with respect to temperature. We deduce in Cao et al. (1995) that the constraint response p maintaining this constraint must appear in both the momentum equation and the energy equation,

$$\rho(\theta)\dot{\boldsymbol{v}} = \operatorname{div}\hat{\boldsymbol{T}} - \operatorname{grad} p + \rho(\theta)\boldsymbol{g}, \tag{2}$$

$$\rho(\theta)\dot{\hat{\epsilon}} + \frac{\rho'(\theta)}{\rho(\theta)}\theta\dot{p} + \frac{p\theta}{\rho(\theta)}\dot{\theta}\left[\rho''(\theta) - 2\frac{\rho'(\theta)^2}{\rho(\theta)}\right] = \hat{\boldsymbol{T}}\cdot\boldsymbol{D} - \operatorname{div}\hat{\boldsymbol{q}}, \tag{3}$$

where $\boldsymbol{g}$ is the acceleration of gravity, $\hat{\boldsymbol{T}}$ the part of the stress tensor given by a constitutive function, $\boldsymbol{D}$ the symmetric part of the velocity gradient, $\hat{\epsilon}$ the constitutive part of internal energy, and $\hat{\boldsymbol{q}}$ the heat flux vector (given by a constitutive assumption). For a material with prescribed temperature-dependent density a term involving the constraint response p, namely $p\theta(\rho'/\rho^2)$, is needed in the internal energy to offset the entropy created by the constraint pressure during thermally induced shrinkage or expansion, so that the net entropy generated by the entire response maintaining the constraint, Eq. 1, is zero.

In this article we explore through solutions of Eqs. 1–3 the behavior of materials with temperature-dependent density in

Correspondence concerning this article should be addressed to S. E. Bechtel.
Present address of Dongbu Cao: Department of Biomedical Engineering/Wb3, The Cleveland Clinic Foundation, 9500 Euclid Avenue, Cleveland, OH 44159.

channel flows with geometries and thermal boundary conditions of practical importance in polymer processing. For such flows the constrained theory, Eqs. 1–3, produces nonlinear two-point boundary-value problems. The solution of each problem was obtained by two independent algorithms, one based on the relaxation method and the other on the shooting method (cf. Press et al., 1992). In all computations the two algorithms converged to the same solution; in the shooting method the stopping criterion was 5×10^{-8} and in the relaxation method the error norm was 5×10^{-6}.

We compare the solutions of Eqs. 1–3 with solutions of an *ad hoc* theory which is the standard practice for accounting for thermal shrinkage, that is, the equations for an incompressible material with *a posteriori* substitution of temperature-dependent density (cf. Hayashi et al., 1992; Dutta, 1987; Kase and Matsuo, 1965),

$$\operatorname{div} \boldsymbol{v} = -\frac{\rho'(\theta)}{\rho(\theta)}\dot{\theta}, \tag{4}$$

$$\rho(\theta)\dot{\boldsymbol{v}} = \operatorname{div}\hat{\boldsymbol{T}} - \operatorname{grad} p + \rho(\theta)\boldsymbol{g}, \tag{5}$$

$$\rho(\theta)\dot{\hat{\epsilon}} = \hat{\boldsymbol{T}}\cdot\boldsymbol{D} - \operatorname{div}\hat{\boldsymbol{q}}. \tag{6}$$

We also compare with solutions of the equations that follow when the density change in the process is ignored and density is treated as a constant ρ_c, equal to $\rho(\theta)$ evaluated at some characteristic temperature:

$$\operatorname{div} \boldsymbol{v} = 0, \tag{7}$$

$$\rho_c\dot{\boldsymbol{v}} = \operatorname{div}\hat{\boldsymbol{T}} - \operatorname{grad} p + \rho_c\boldsymbol{g}, \tag{8}$$

$$\rho_c\dot{\hat{\epsilon}} = \hat{\boldsymbol{T}}\cdot\boldsymbol{D} - \operatorname{div}\hat{\boldsymbol{q}}. \tag{9}$$

To complete the boundary-value problem formulation for a material with temperature-dependent density for any of the theories, Eqs. 1–3, 4–6, or 7–9, we must specify the density function $\rho(\theta)$ or effective constant ρ_c, the constitutive functions $\hat{\boldsymbol{T}}$, $\hat{\epsilon}$, and $\hat{\boldsymbol{q}}$ for the determinate parts of stress, internal energy, and heat flux, respectively, the body force $\boldsymbol{g}$, and the mechanical and thermal boundary conditions for the process. Our constitutive assumptions for internal energy and heat flux are

$$d\hat{\epsilon} = c\,d\theta, \qquad \hat{\boldsymbol{q}} = -k\operatorname{grad}\theta. \tag{10}$$

To focus on the effect of temperature dependence of density we consider the specific heat c and thermal conductivity k as constants, although Eqs. 1–3 are valid with c and k taken as functions of temperature. We employ the Newtonian model for stress with an Arrhenius form for viscosity,

$$\hat{\boldsymbol{T}} = 2\mu(\theta)\boldsymbol{D}, \qquad \mu(\theta) = \mu_c \exp\left[\frac{\mathcal{E}}{R}\left(\frac{1}{\theta}-\frac{1}{\theta_c}\right)\right], \tag{11}$$

where the constants $\mathcal{E}$, R, and θ_c are the activation energy, gas constant, and a characteristic temperature, respectively, and μ_c is the viscosity at the characteristic temperature. For specificity, we assume a linear dependence of density on temperature,

$$\rho(\theta) = \rho_0 - \rho_1\theta, \tag{12}$$

where ρ_0 and ρ_1 are constants.

In Cao et al. (1995), as a demonstration of the constrained theory we present solutions for plane Poiseuille flow with isothermal walls. Here we present solutions for plane Poiseuille, capillary, and annular flows subject to industrially relevant thermal boundary conditions.

Plane Poiseuille Flows

As our first geometry, we investigate flows between two infinite planar surfaces with separation d (Figure 1). Consistent with our adoption of the Newtonian constitutive model for the fluid, at the walls we impose the mechanical boundary condition of no slip,

$$\boldsymbol{v} = \boldsymbol{0} \qquad \text{at} \qquad x_2 = \pm\frac{d}{2}. \tag{13}$$

As the thermal boundary condition we impose

$$\frac{\partial\theta}{\partial x_2} = h(\theta-\theta_c) \qquad \text{at} \qquad x_2 = \pm\frac{d}{2}, \tag{14}$$

where θ_c is a specified constant die temperature, x_2 is the transverse Cartesian coordinate, and h is a constant heat loss coefficient. This condition has two limiting cases: when $h = 0$ the walls are adiabatic (i.e., perfectly insulated),

$$\frac{\partial\theta}{\partial x_2} = 0 \qquad \text{at} \qquad x_2 = \pm\frac{d}{2}, \tag{15}$$

and there is no heat flow from the fluid into the walls; when $1/h = 0$, the walls are isothermal,

$$\theta = \theta_c \qquad \text{at} \qquad x_2 = \pm\frac{d}{2}, \tag{16}$$

so that energy is supplied externally to maintain a specified fluid temperature near the walls.

We seek solutions that are steady, two-dimensional, laminar, and hydrodynamically and thermally fully developed, so that with the coordinate directions defined as in Figure 1 the velocity and temperature fields are of the form

$$v_1 = v_1(x_2), \quad v_2 = 0, \quad v_3 = 0, \quad \theta = \theta(x_2). \tag{17}$$

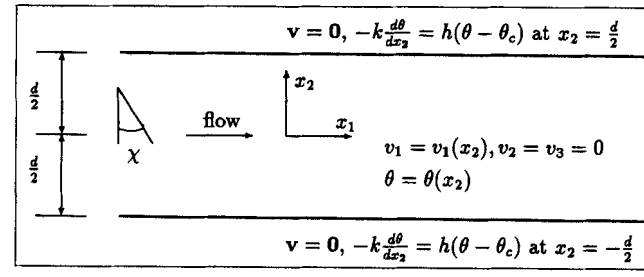

Figure 1. Fully developed plane Poiseuille flow.

For such a solution to exist in the presence of gravity the channel must be oriented so that the x_1, x_2 plane is vertical, that is, the body force per unit mass must be in the x_1, x_2 plane:

$$g = g(\sin\chi e_1 - \cos\chi e_2), \tag{18}$$

where g is the magnitude of the acceleration of gravity and χ is the angle the flow (x_1) direction is depressed from horizontal.

Constrained theory

We first model the plane Poiseuille flow of Figure 1 with the thermomechanically constrained theory, Eqs. 1–3. To nondimensionalize the boundary-value problem, we scale temperature to the die temperature θ_c, length to the wall separation d, and velocity to $v_0 = (\beta d^2/8\mu_c)$, the maximum velocity in isothermal plane Poiseuille flow with an applied pressure gradient β and viscosity $\mu_c = \mu(\theta_c)$. Hence, the dimensionless transverse coordinate, temperature, and velocity are

$$\tilde{x}_2 = \frac{x_2}{d}, \quad \tilde{\theta} = \frac{\theta}{\theta_c}, \quad \tilde{v}_1 = \frac{v_1}{v_0} = \frac{8\mu_c v_1}{\beta d^2}. \tag{19}$$

Using the material density at the die temperature, $\rho_c = \rho(\theta_c)$, as the characteristic value of density, the dimensionless form of the density function, Eq. 12, becomes

$$\tilde{\rho}(\tilde{\theta}) = \frac{\rho(\theta)}{\rho_c} = \frac{1 - P\tilde{\theta}}{1 - P}, \qquad P = \frac{\rho_1\theta_c}{\rho_0}, \tag{20}$$

where the dimensionless thermal expansion number P is a measure of the degree of temperature dependence of the material's density at the processing conditions.

The boundary-value problem for fully developed plane Poiseuille flow reduces to the dimensionless equations

$$\frac{d^2\tilde{v}_1}{d\tilde{x}_2^2} - \frac{E}{\tilde{\theta}^2}\frac{d\tilde{\theta}}{d\tilde{x}_2}\frac{d\tilde{v}_1}{d\tilde{x}_2} = -\left[8 + \frac{1 - P\tilde{\theta}}{1 - P}G\right]\exp\left[-E\left(\frac{1}{\tilde{\theta}} - 1\right)\right], \tag{21}$$

$$\frac{d^2\tilde{\theta}}{d\tilde{x}_2^2} = -64\mathrm{Br}\tilde{x}_2^2\exp\left[-E\left(\frac{1}{\tilde{\theta}} - 1\right)\right] + 8\mathrm{Br}P\frac{\tilde{v}_1\tilde{\theta}}{1 - P\tilde{\theta}}, \tag{22}$$

subject to the boundary conditions

$$\tilde{v}_1 = 0, \quad \frac{d\tilde{\theta}}{d\tilde{x}_2} = \mathrm{Bi}(1 - \tilde{\theta}) \quad \text{at} \quad \tilde{x}_2 = \pm\frac{1}{2}. \tag{23}$$

In Eqs. 21–23,

$$\mathrm{Br} = \frac{\beta^2 d^4}{64k\mu_c\theta_c} = \frac{\tau_w^2 d^2}{16k\mu_c\theta_c}, \qquad E = \frac{\mathcal{E}}{R\theta_c},$$

$$\mathrm{Bi} = \frac{hd}{k}, \qquad G = \frac{8\rho_c g\sin\chi}{\beta} = \frac{4\rho_c g d\sin\chi}{\tau_w}, \tag{24}$$

where the absolute value τ_w of shear stress at the wall is related to the pressure gradient β by $\tau_w = (1/2)\beta d$. Br is the Brinkman number indicating the balance of the competing effects of viscous heating and thermal conduction, E is the Arrenhius number, Bi is the Biot number, and G is the Gallileo number. The term $8\mathrm{Br}P(\tilde{v}_1\tilde{\theta}/(1 - P\tilde{\theta}))$ in Eq. 22 is the constraint response in the energy equation; it is through this term that the energy equation, Eq. 22, couples to the momentum equation, Eq. 21. In all computations we will assume the die walls are horizontal, so that $G = 0$.

Ad hoc and constant-density theories

If the plane Poiseuille flow shown in Figure 1 is modeled with the *ad hoc* theory, Eqs. 4–6 (in which a temperature-dependent density function is substituted *a posteriori* in the incompressible equations), the dimensionless problem reduces to the equations

$$\frac{d^2\tilde{v}_1}{d\tilde{x}_2^2} - \frac{E}{\tilde{\theta}^2}\frac{d\tilde{\theta}}{d\tilde{x}_2}\frac{d\tilde{v}_1}{d\tilde{x}_2} = -\left[8 + \frac{1 - P\tilde{\theta}}{1 - P}G\right]\exp\left[-E\left(\frac{1}{\tilde{\theta}} - 1\right)\right], \tag{25}$$

$$\frac{d^2\tilde{\theta}}{d\tilde{x}_2^2} = -64\mathrm{Br}\tilde{x}_2^2\exp\left[-E\left(\frac{1}{\tilde{\theta}} - 1\right)\right], \tag{26}$$

subject to the boundary conditions, Eq. 23. Note that Eq. 26 for the temperature distribution decouples from the equation for velocity, Eq. 25.

If the plane Poiseuille flow is modeled with Eqs. 7–9 (in which the density is treated as constant), the problem reduces to

$$\frac{d^2\tilde{v}_1}{d\tilde{x}_2^2} - \frac{E}{\tilde{\theta}^2}\frac{d\tilde{\theta}}{d\tilde{x}_2}\frac{d\tilde{v}_1}{d\tilde{x}_2} = -(8 + G)\exp\left[-E\left(\frac{1}{\tilde{\theta}} - 1\right)\right], \tag{27}$$

$$\frac{d^2\tilde{\theta}}{d\tilde{x}_2^2} = -64Br\tilde{x}_2^2\exp\left[-E\left(\frac{1}{\tilde{\theta}} - 1\right)\right]. \tag{28}$$

For simulations of flow between horizontal planes, $G = 0$ and both Eqs. 25 and 26 and Eqs. 27 and 28 collapse to

$$\frac{d\tilde{v}_1}{d\tilde{x}_2} = -8\tilde{x}_2\exp\left[-E\left(\frac{1}{\tilde{\theta}} - 1\right)\right], \tag{29}$$

$$\frac{d^2\tilde{\theta}}{d\tilde{x}_2^2} = -64\mathrm{Br}\tilde{x}_2^2\exp\left[-E\left(\frac{1}{\tilde{\theta}} - 1\right)\right]. \tag{30}$$

An important conclusion from Eqs. 29 and 30 is that even though the *ad hoc* theory considers density as a function of temperature, it does so in such a way that if the die walls are

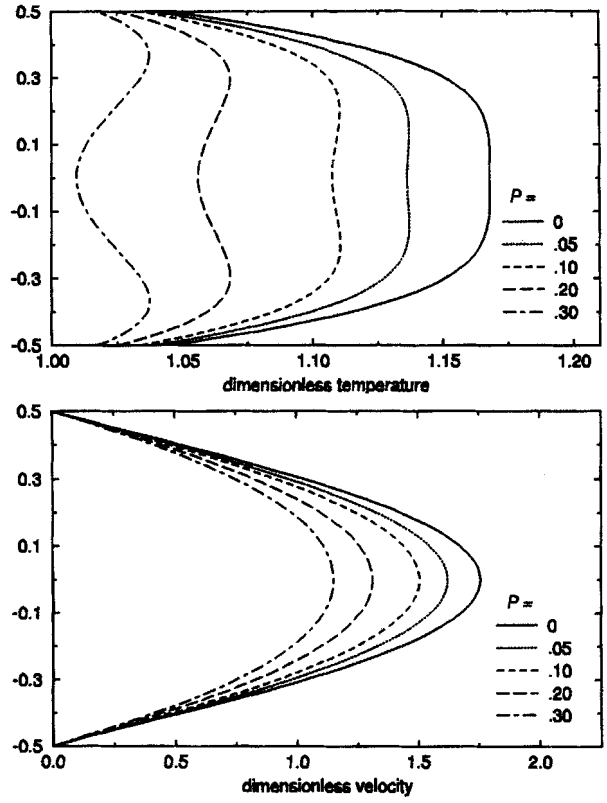

Figure 2. Velocity and temperature distributions in non-isothermal plane Poiseuille flows predicted by the constrained theory, varying the level of temperature dependence of density.

$E = 5.0$, Br = 0.2, Bi = 20, variable P. The vertical coordinate is the dimensionless transverse coordinate $\tilde{x}_2$.

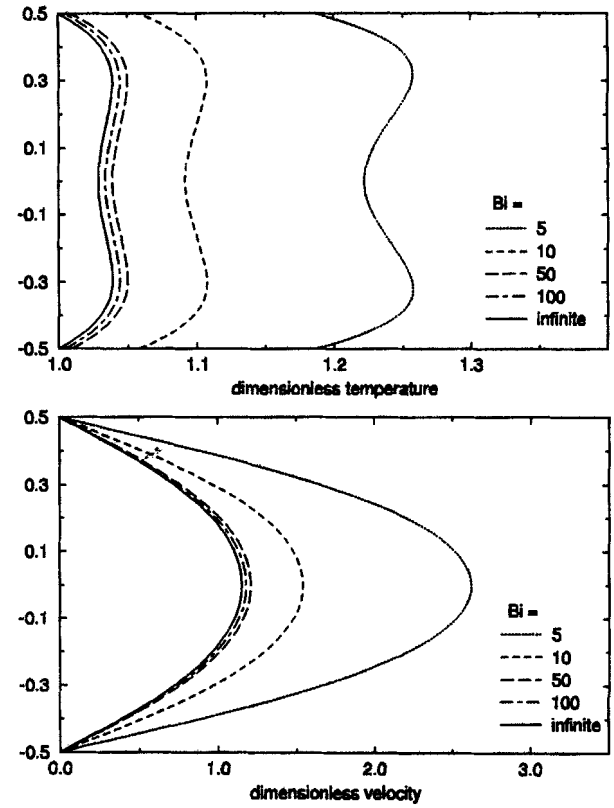

Figure 3. Velocity and temperature distributions in non-isothermal plane Poiseuille flows predicted by the constrained theory, varying the heat-loss boundary condition at the die walls.

$E = 5.0$, Br = 0.2, $P = 0.2$, variable Bi.

horizontal (or if gravity is neglected) the temperature dependence of density has no effect on velocity and temperature, since the parameter P is absent from Eqs. 29 and 30.

Predictions of the constrained theory

Figure 2 shows the effect of temperature dependence of density predicted by the constrained theory. It exhibits the features discovered in Cao et al. (1995): if there is a nonzero thermal expansion coefficient ($P \neq 0$), the solution exhibits expansion cooling and an overall decrease in the velocity. Expansion cooling is the phenomenon of depressed temperature in the center of the channel, due to the competing effects of viscous heating and thermal expansion. The fluid interior undergoes viscous heating, which tends to increase fluid temperature in the center; this heating also tends to expand the fluid, and the work done in this expansion leads to a decrease of temperature.

The effect of thermal boundary condition $(23)_2$ on the velocity and temperature fields is shown in Figures 3 and 4, where velocity and temperature distributions are plotted for fixed E, Br, and P with varying Bi (which can be accomplished by changing the heat-loss coefficient h and holding all other flow conditions and material properties constant). Figure 3 displays values of the Biot number approaching the isothermal wall limit, and Figure 4 displays values approaching the adiabatic wall limit.

The solutions for large Biot numbers smoothly approach the solution for the isothermal wall case ($1/h = 0$, Bi $\to \infty$), as witnessed in Figure 3. As Bi decreases from this limit, the bulk temperature, temperature near the wall, and velocity of the fluid all increase, and the expansion cooling phenomenon of depressed temperature in the center of the channel becomes more pronounced.

For Bi near zero the effect of expansion cooling is to maintain a center temperature in steady flows that is insensitive to Bi, even as the fluid temperature near the walls and the average fluid velocity becomes large when Bi $\to 0$ (Figure 4). For flows in slit dies with adiabatic walls ($h = 0$, Bi = 0), fully developed flow conditions are not possible.

Another effect of the finite value of heat-loss coefficient h in the thermal boundary condition $(23)_2$ is the possibility of multiple solutions of the governing equations, Eqs. 25 and 26. To see this, we now investigate the dimensionless mass-flow rate,

$$\int_0^1 \tilde{\rho}\tilde{v}_1 \, d\tilde{x}_2 = \int_0^1 \frac{1 - P\tilde{\theta}(\tilde{x}_2)}{1 - P} \tilde{v}_1(\tilde{x}_1) \, d\tilde{x}_2, \qquad (31)$$

as a function of the expansion number P and Biot number Bi. Figure 5 plots dimensionless mass-flow rate vs. P for fixed values of Bi. At some values of Biot number there is a range of P for which the curve has two branches, indicating two

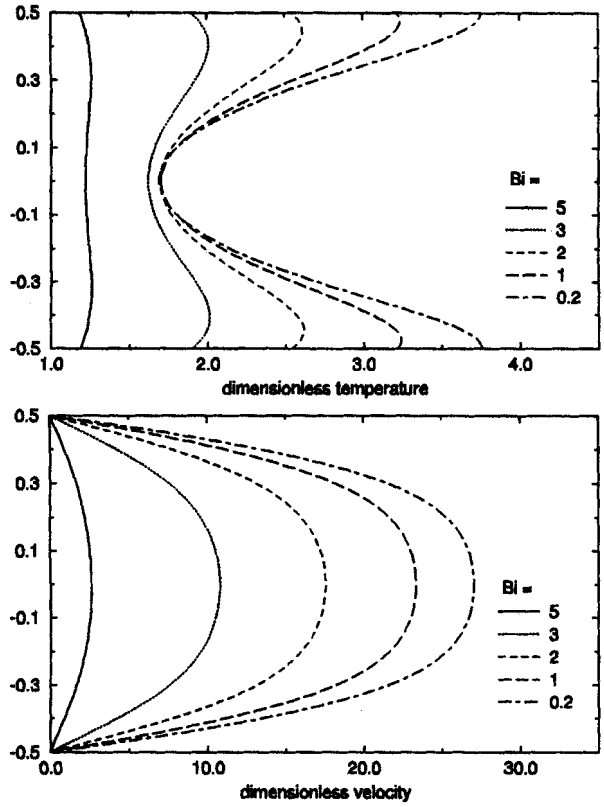

Figure 4. Velocity and temperature distributions in non-isothermal plane Poiseuille flows predicted by the constrained theory, varying the heat-loss boundary condition at the die walls.

$E = 5.0$, Br = 0.2, $P = 0.2$, variable Bi.

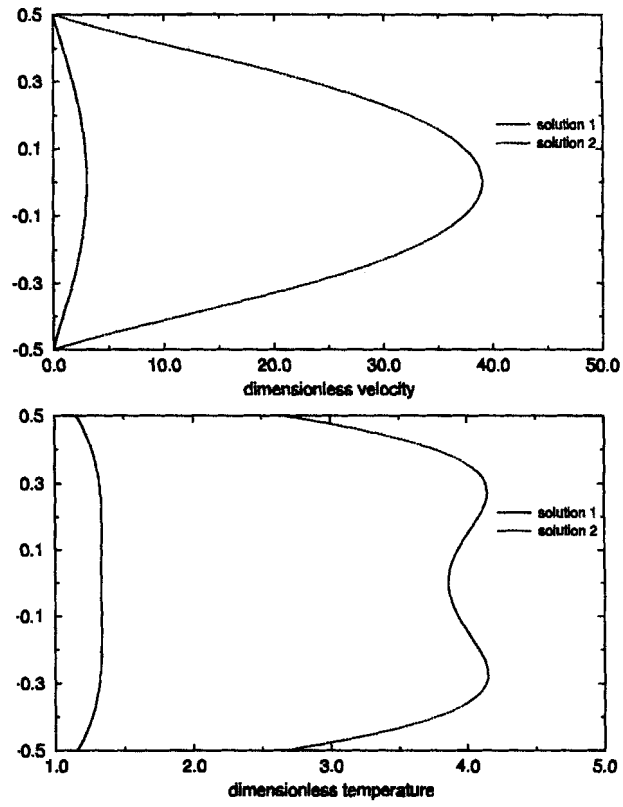

Figure 6. Multiple solutions for the velocity and temperature distributions predicted by the constrained theory.

$E = 5.0$, Br = 0.2, $P = 0.05$, Bi = 9.0.

solutions. From an extensive parameter study we learned the following (we restrict to Bi and P nonnegative):

- For Bi less than 6.3 and greater than 20.1 the solutions for velocity and temperature are single-valued for all values of P.
- If Bi is between 6.3 and 20.1, there is a bounded range of P in which two solution pairs of $[\tilde{v}_1(\tilde{x}_2), \tilde{\theta}(\tilde{x}_2)]$ exist. At Bi = 6.3 this range is very narrow, $0.1140 < P < 0.1142$. As Bi increases, this range of P becomes wider and shifts toward $P = 0$, until at Bi = 10.3 the range of P for multiple solutions

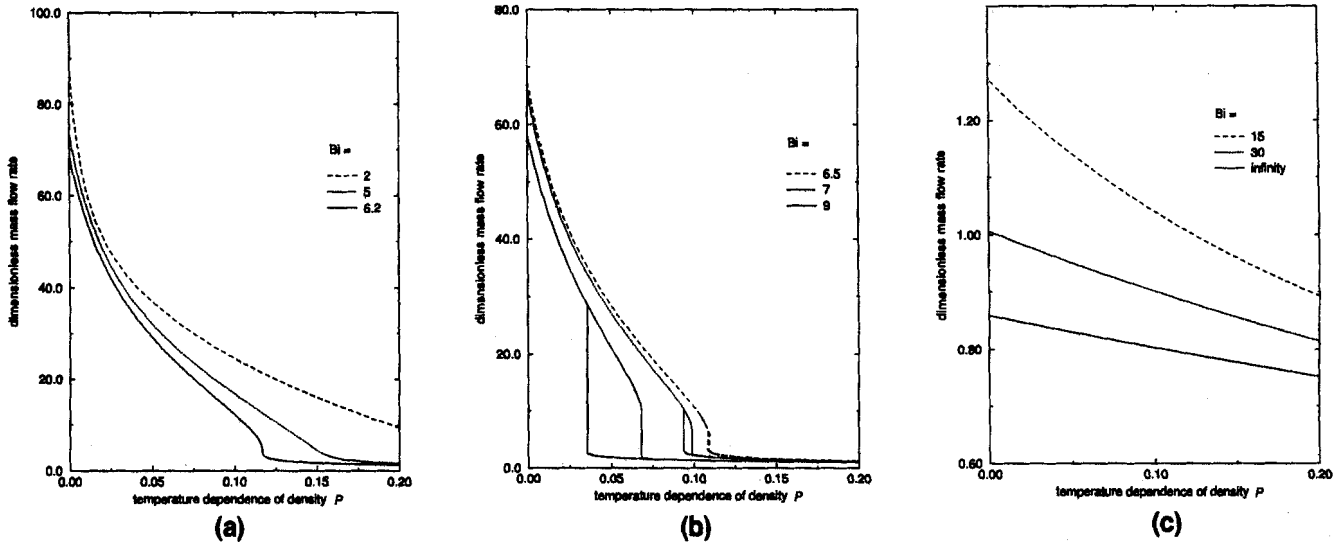

Figure 5. Dimensionless mass-flow rate as a function of the level of temperature dependence of density, for differing heat-loss boundary conditions at the die walls: prediction of the constrained theory.

$E = 5.0$, Br = 0.2, variable Bi.

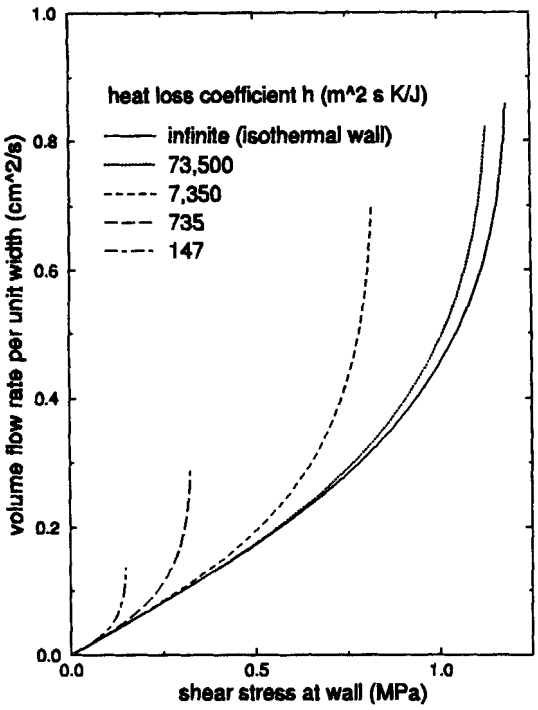

Figure 7. Effect of the heat-loss condition at the die walls on the relation between volume flow rate per unit width of the channel and wall shear stress for the PET melt flows of Table 1.

Predictions of the constrained theory.

includes $P = 0$ (explicitly, $0 \le P < 0.0535$). By Bi = 20.1 the range of P has shifted entirely out of the nonnegative P domain.

In Figure 6 we simulate a process for which Eqs. 25 and 26 have two solutions. None of the simulations presented in Figures 2–4 are in the preceding ranges for multiple solutions to exist, so that Figures 2–4 exhibit unique solutions of Eqs. 25 and 26.

We now investigate a particular family of processes of a material that is commonly modeled with the Newtonian constitutive model, Eq. 11, and the linear dependence, Eq. 12, of density on temperature, and obtain predictions of dimensional volume flow rates. We simulate flows in which poly(ethylene terephatalate) (PET) is melt processed in a steady plane Poiseuille flow with a wall separation of 0.2 mm and die temperature θ_c of 285°C (Table 1). For these processes the Arrenhius number E is 12.18 and the expansion number P is 0.1869 (this value of P eliminates the possibility of multiple solutions). The Brinkman and Biot numbers are functions of wall stress τ_w (or equivalently the imposed pressure gradient $\beta = (2\tau_w/d)$) and heat loss coefficient h, respectively, which are treated as variables in our parameter study. Figure 7 demonstrates how the heat-loss condition at the die walls influences the relation between volume flow rate per unit width of the channel and wall shear stress. We observe that at a fixed wall stress the volume flow rate increases as the heat-loss coefficient decreases.

The volume flow rate vs. wall shear stress curves in Figure 7 terminate at critical values of shear stress τ_w; up to these values both the algorithm based on the relaxation method and the algorithm based on the shooting method converge to the same solutions, and beyond them neither algorithm converges. We conjecture that this is indicative of the onset of a physical instability in the flow as seen by Martin (1967) and Sukanek (1971). The loss of convergence occurs at lower values of τ_w as the heat-loss coefficient decreases.

Table 1. PET Properties and Flow Conditions Used in the Plane Poiseuille Flow Simulations, and Corresponding Dimensionless Numbers

Material properties for PET		
Density coefficient ρ_0	1,493	$kg \cdot m^{-3}$*
Density coefficient ρ_1	0.5	$kg \cdot m^{-3} \cdot K^{-1}$*
Thermal conductivity k	0.147	$W \cdot m^{-1} \cdot K^{-1}$†
Intrinsic viscosity $[\eta]$	0.6450	$dL \cdot g^{-1}$†
Activation energy $\mathcal{E}$	56.54×10^3	$J \cdot mol^{-1}$*
Flow conditions		
Wall separation d	0.2	mm
Die temperature θ_c	285	°C = 558.2 K
Viscosity μ_c at die temp.	204.6	Pa·s‡
Shear stress at wall τ_w	Variable	
Heat-loss coefficient h	Variable	
Dimensionless numbers		
Arrhenius number E	12.18	
Brinkman number $Br = Br(\tau_w)$	$0.1489\tau_w^2$	MPa^{-2}
Expansion number P	0.1869	
Biot number $Bi = Bi(h)$	$0.001361h$	$J \cdot m^{-2} \cdot s^{-1} \cdot K^{-1}$

*Hayashi et al. (1992).
†Brandrup and Immergut (1989).
‡Calculated by $\mu(\theta) = [\eta]^{5.15} \exp\{(\mathcal{E}/R\theta) - 2.3\}$ poise.

Comparison with the ad hoc and constant-density theories

In this subsection we compare the predictions of the constrained, *ad hoc*, and constant-density theories. The predictions of the *ad hoc* and constant-density theories for temperature, velocity, and volume flow rates are identical, since as noted earlier the governing equations for temperature and velocity from these theories collapse for flows between horizontal walls to the same Eqs. 29 and 30. The constrained, *ad hoc*, and constant-density theories produce distinct predictions only for mass-flow rate.

Corresponding to Figure 2, the velocity and temperature profiles predicted by the *ad hoc* theory for flows with varying levels of temperature dependence of density are identical to those of the constant-density theory and given by the $P = 0$ curves in Figure 2. Because the constraint response term is missing from the internal energy, the *ad hoc* theory cannot model expansion cooling, and predictions for velocity and temperature are unaffected by thermal expansion and too large. Hence, for $P \neq 0$ and any value of Bi, the *ad hoc* theory makes both qualitative and quantitative errors in the velocity and temperature. We now investigate the dependence of the magnitudes of these errors on the heat-loss boundary condition at the die walls. Compare Figure 8 to Figure 3, and Figure 9 to Figure 4. All three theories predict that the polymer temperature near the walls, average velocity, and maximum (midchannel) velocity blow up as Bi nears zero (reflecting that no steady solution exists for the case of adiabatic walls), but the increase happens with Bi much farther away from zero with the *ad hoc* and constant-density theories. For Bi = 10, from Figure 3 we see that the polymer temperature

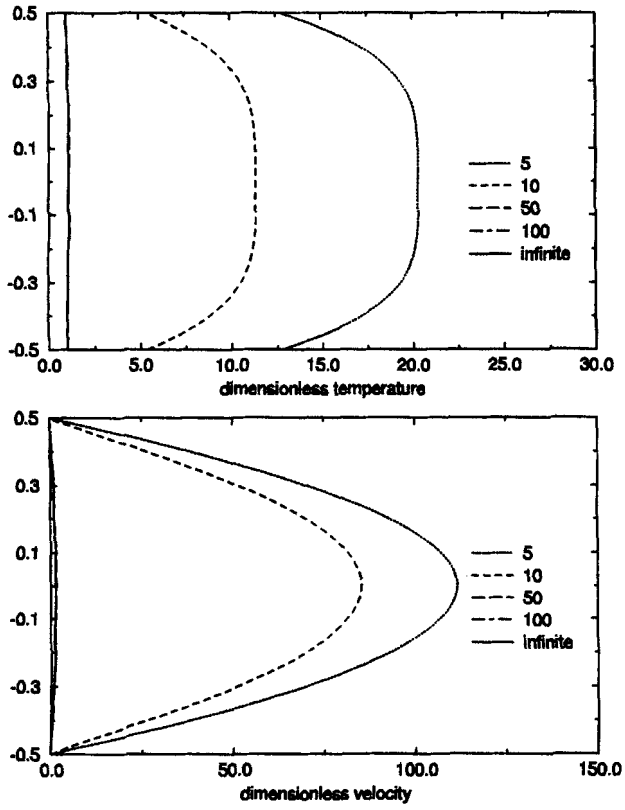

Figure 8. Velocity and temperature distributions in non-isothermal plane Poiseuille flows predicted by the *ad hoc* and constant-density theories, varying the heat-loss boundary condition at the die walls.

$E = 5.0$, Br = 0.2, $P = 0.2$, variable Bi. The vertical coordinate is the dimensionless transverse coordinate $\tilde{x}_2$.

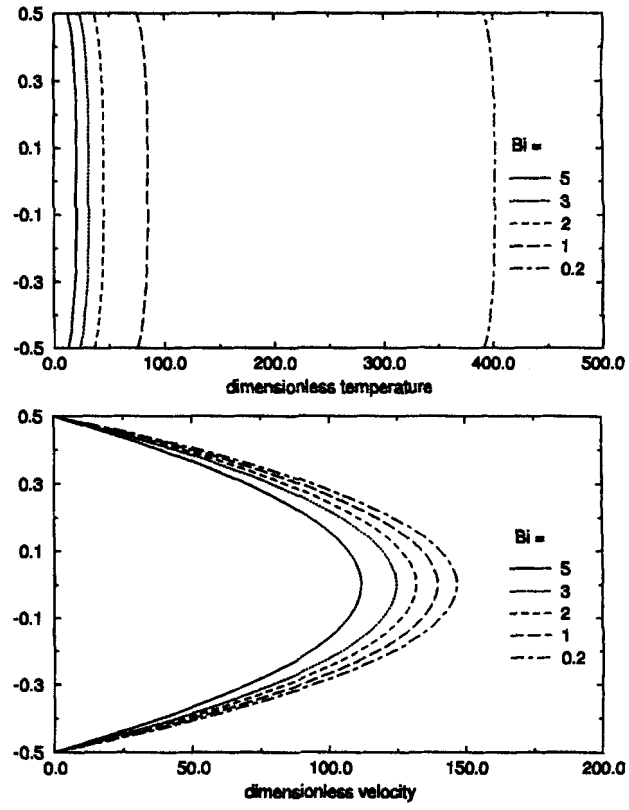

Figure 9. Velocity and temperature distributions in non-isothermal plane Poiseuille flows predicted by the *ad hoc* and constant-density theories, varying the heat-loss boundary condition at the die walls.

$E = 5.0$, Br = 0.2, $P = 0.2$, variable Bi.

near the wall predicted by the constrained theory is 1.06 times the die temperature and the dimensionless midchannel velocity is 1.54, whereas from Figure 8 we see that the corresponding numbers predicted by the *ad hoc* and constant-density theories are 5.38 and 85.2, respectively. For Bi = 0.2 the same quantities are 3.75 and 27.1 from the constrained theory (Figure 4) and 392 and 146 from the ad hoc and constant-density theories (Figure 9). The effect of expansion cooling to hold the midchannel temperature near 1.7 times the die temperature as Bi $\rightarrow$ 0 (Figure 4) is not captured by the ad hoc and constant-density theories (Figure 9).

Figure 10 compares the dimensionless mass-flow rates predicted by the three theories. Although the *ad hoc* and constant-density theories produce identical temperature and velocity profiles, they predict different density profiles [$\tilde{\rho}(\tilde{x}_2) = [1 - P\tilde{\theta}(\tilde{x}_2)]/(1 - P)$ in the *ad hoc* theory and $\tilde{\rho}(\tilde{x}_2) = 1$ in the constant density theory], and hence different mass-flow rates $\int_0^1 \tilde{\rho}\tilde{v}_1 \, d\tilde{x}_2$. For $P \neq 0$ the *ad hoc* theory overpredicts the velocity, tending to an overprediction of mass-flow rate, but also overpredicts the polymer temperature and hence underpredicts the density, tending to an underprediction of mass-flow rate. The net result of these competing errors is an overprediction of mass-flow rate for large Bi and an underprediction for small Bi. In fact, for small enough Bi and large enough P the overprediction of polymer temperature by the *ad hoc* theory is so great that the approximation $\tilde{\rho}(\tilde{x}_2) = [1 - P\tilde{\theta}(x_2)]/(1 - P)$ of a linear dependence of density on temperature results in a negative density and a negative mass-flow rate. The constant-density theory overpredicts the mass-flow rate for all values of P and Bi.

Figure 11 compares the volume flow rate vs. wall shear stress predicted by the constrained theory and *ad hoc* theory (equivalent to the prediction of the constant-density theory) for the processes of Table 1. Both the constrained and *ad hoc* theories predict that at fixed wall stress the volume flow rate increases as the heat-loss coefficient decreases, but at any value of h the *ad hoc* theory overestimates the flow rate: for example, when $\tau_w = 0.635$ MPa (Br = 0.0600) and $h =$ 7,350 $m^2 \cdot K/J$ (Bi = 10.0), the constrained and *ad hoc* theories predict volume flow rates per unit width of 0.285 and 0.383 cm^2/s, respectively. The curves for both the constrained theory and *ad hoc* theory cease at the values of wall stress beyond which neither of the solution algorithms converge. Again we conjecture that beyond these values no stable solutions to the boundary-value problems exist. For a given h this limiting value is less in the *ad hoc* theory than in the constrained theory; for example, when $h = 735$ $m^2 \cdot K/J$ (Bi = 1.00) it is 0.276 MPa for the *ad hoc* theory and 0.325 MPa for the constrained theory.

Capillary Flows

As our second geometry we consider fully developed tor-

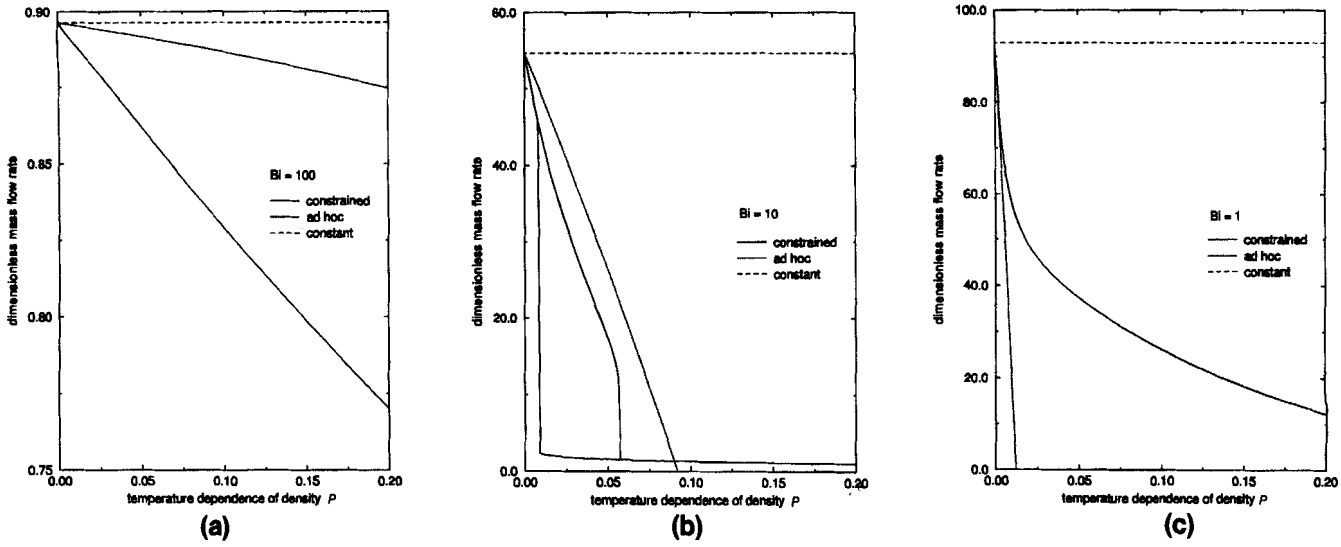

Figure 10. Dimensionless mass-flow rate as a function of the level of temperature dependence of density for differing heat-loss boundary conditions at the die walls.

Comparison of the constrained, *ad hoc*, and constant-density theories. $E = 5.0$, Br = 0.2, variable Bi.

sionless flows in circular conduits, as in a spinneret die. In this and the following sections we neglect gravity. We employ cylindrical coordinates (r, ϕ, z) with the z-axis in the flow direction, and denote the radius of the capillary by r_0 (see Figure 12). At the capillary wall we impose no slip,

$$\boldsymbol{v} = \mathbf{0} \qquad \text{at} \qquad r = r_0, \tag{32}$$

and the heat loss condition

$$-k\frac{\partial\theta}{\partial r} = h(\theta - \theta_c), \qquad \text{at} \qquad r = r_0. \tag{33}$$

For the fully developed torsionless flow we have

$$v_z = v_z(r), \qquad v_r = v_\psi = 0, \qquad \theta = \theta(r). \tag{34}$$

The constrained theory

The dimensionless boundary-value problem for the fully developed capillary flow of Figure 12 as modeled by the thermomechanically constrained theory, Eqs. 1–3, reduces to

$$\frac{d\tilde{v}_z}{d\tilde{r}} = -2\tilde{r}\exp\left[-E\left(\frac{1}{\tilde{\theta}} - 1\right)\right], \tag{35}$$

$$\frac{d^2\tilde{\theta}}{d\tilde{r}^2} + \frac{1}{\tilde{r}}\frac{d\tilde{\theta}}{d\tilde{r}} = -\mathrm{Br}\tilde{r}^2\exp\left[-E\left(\frac{1}{\tilde{\theta}} - 1\right)\right] + \mathrm{Br}P\frac{\tilde{v}_z\tilde{\theta}}{1 - P\tilde{\theta}}, \tag{36}$$

subject to the symmetry conditions

$$\frac{d\tilde{v}_z}{d\tilde{r}} = 0, \qquad \frac{d\tilde{\theta}}{d\tilde{r}} = 0 \qquad \text{at} \qquad \tilde{r} = 0, \tag{37}$$

at the centerline, and the no-slip and heat-loss conditions

$$\tilde{v}_z = 0, \qquad \frac{d\tilde{\theta}}{d\tilde{r}} = \mathrm{Bi}(1 - \theta) \qquad \text{at} \qquad \tilde{r} = 1, \tag{38}$$

at the wall. In Eqs. 35–38, we have scaled the problem according to

$$\tilde{r} = \frac{r}{r_0}, \qquad \tilde{\theta} = \frac{\theta}{\theta_c}, \qquad \tilde{v}_z = \frac{4\mu_c v_z}{\beta r_0^2}, \tag{39}$$

and the dimensionless groups are now defined

$$\mathrm{Br} = \frac{\beta^2 r_0^4}{4k\mu_c\theta_c} = \frac{\tau_w^2 r_0^2}{k\mu_c\theta_c}, \qquad \mathrm{Bi} = \frac{hr_0}{k},$$

$$E = \frac{\mathcal{E}}{R\theta_c}, \qquad P = \frac{\rho_1\theta_c}{\rho_0}. \tag{40}$$

The shear stress τ_w at the wall of the capillary is related to the applied pressure gradient β by $\tau_w = (1/2)\beta r_0$.

Ad hoc and constant-density theories

If the same capillary flow shown in Figure 12 is modeled with either the *ad hoc* theory, Eqs. 4–6 (in which a temperature-dependent density function is substituted *a posteriori* in the incompressible equations) or the constant-density theory, Eqs. 7–9, the dimensionless problem reduces to

$$\frac{d\tilde{v}_z}{d\tilde{r}} = -2\tilde{r}\exp\left[-E\left(\frac{1}{\tilde{\theta}} - 1\right)\right], \tag{41}$$

$$\frac{d^2\tilde{\theta}}{d\tilde{r}^2} + \frac{1}{\tilde{r}}\frac{d\tilde{\theta}}{d\tilde{r}} = -\mathrm{Br}\tilde{r}^2\exp\left[-E\left(\frac{1}{\tilde{\theta}} - 1\right)\right], \tag{42}$$

subject to the boundary conditions, Eqs. 37 and 38. Note that

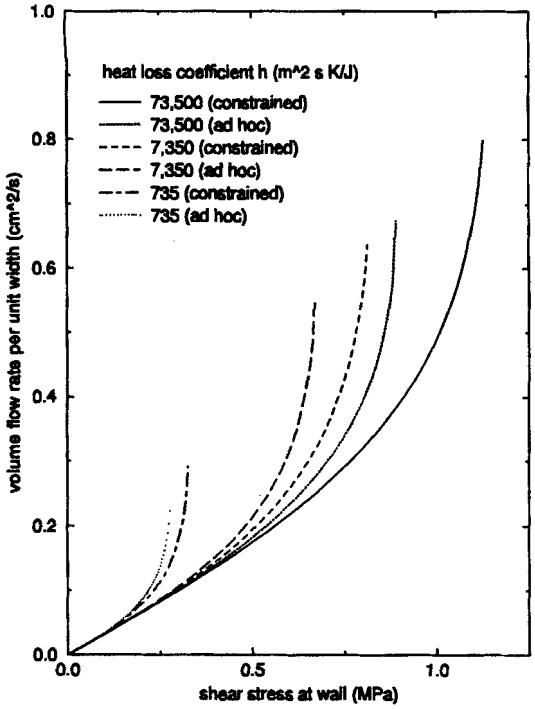

Figure 11. Effect of the heat-loss condition at the die walls on the relation between volume flow rate per unit width of the channel and wall shear stress for the PET melt flows of Table 1.

Comparison between the predictions of the constrained and *ad hoc* theories.

Eq. 42 for temperature decouples from Eq. 41 for velocity, and the temperature dependence of density, although inserted in the theory, has no effect on the temperature and velocity distributions (since P is absent from Eqs. 41 and 42).

Predictions of the constrained theory

As with plane flows, capillary and annular flows have the possibility of multiple solutions, but we only perform simulations that have unique solutions. The effect of temperature-dependent density on velocity and temperature in a capillary flow is shown in Figure 13. As noted in compressible analyses of capillary flows (Duda et al., 1988; Winter, 1975), the temperature profile has a broad, flat plateau in the center of the capillary, due to expansion cooling. A comparison of Figure 13 to Figure 2 shows that this depression of temperature occupies proportionately more of the channel in the capillary flow than in the corresponding slit die flow, with sharper temperature gradients confined to a smaller layer near the die wall. Also, the capillary flow exhibits significantly less sensitivity of velocity to the temperature dependence of density than the slit die flow.

The effect on velocity and temperature of varying the heat loss condition $(38)_2$ is shown in Figures 14 and 15. The rate of increase of temperature and velocity with decreasing Bi is less than in plane Poiseuille flow (compare Figures 14 and 15 to Figures 3 and 4), although as in the plane Poiseuille case the temperature and velocity become unbounded as Bi $\rightarrow$ 0.

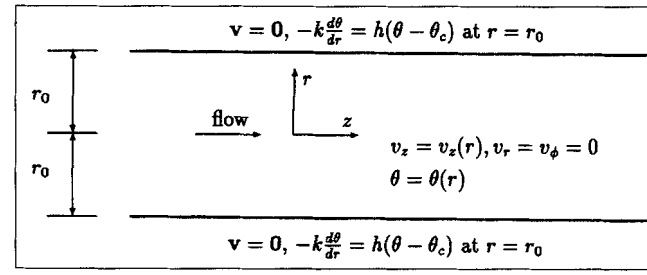

Figure 12. Fully developed capillary flow.

Note from Figure 15 that as Bi becomes small, the midconduit temperature is not held constant, independent of Bi, as in plane Poiseuille flow (Figure 4).

Figure 16 shows the influence of the heat-loss boundary condition at the wall on the relation between volume flow rate and wall shear stress for the PET melt flows of Table 2 (the material properties of PET are listed in Table 1). As in plane Poiseuille flow (Figure 7) we observe that at a fixed wall stress τ_w the volume flow rate increases as the heat-loss coefficient h decreases, and the value of τ_w beyond which there are no stable solutions decreases with h.

Comparison with the ad hoc and constant-density theories

The velocity and temperature profiles predicted by the *ad*

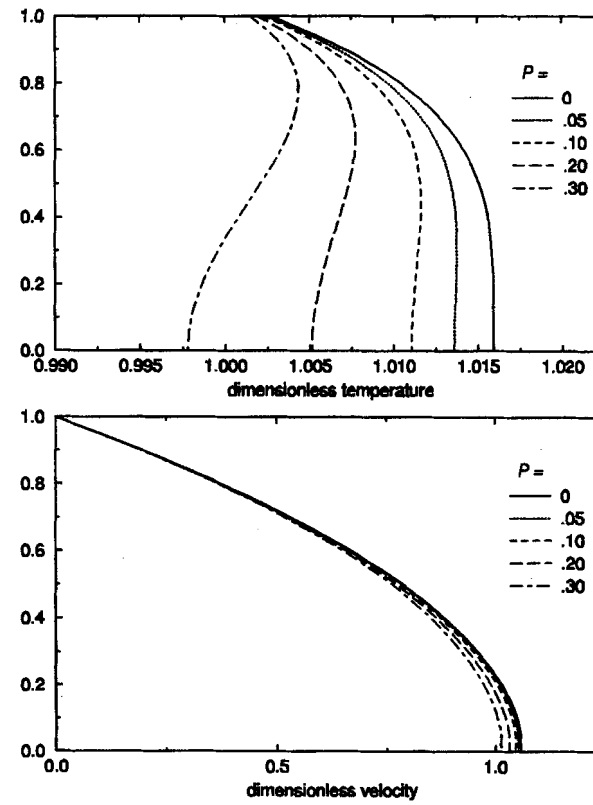

Figure 13. Velocity and temperature distributions in nonisothermal capillary flows predicted by the constrained theory, varying the level of temperature dependence of density.

$E = 5.0$, Br = 0.2, Bi = 20, variable P. The vertical coordinate is the dimensionless transverse coordinate $\tilde{r}$, where $\tilde{r} = 0$ is the centerline of the pipe.

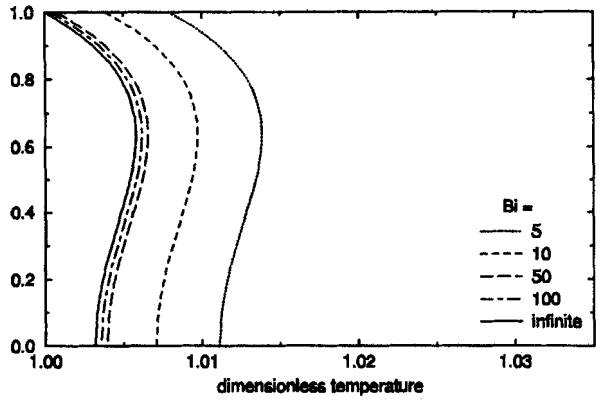

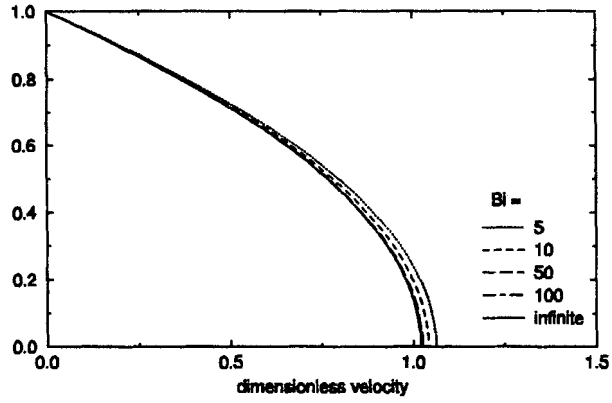

Figure 14. Velocity and temperature distributions in nonisothermal capillary flows predicted by the constrained theory, varying the heat-loss boundary condition at the die wall.

$E = 5.0$, Br = 0.2, $P = 0.2$, variable Bi.

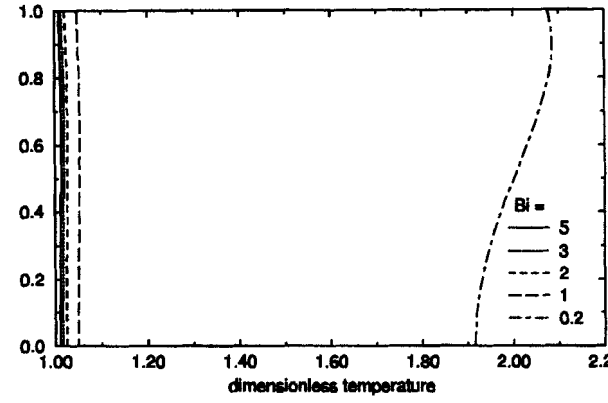

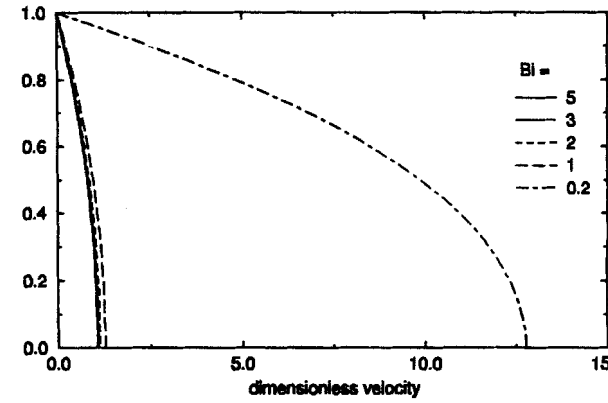

Figure 15. Velocity and temperature distributions in nonisothermal capillary flows predicted by the constrained theory, varying the heat-loss boundary condition at the die wall.

$E = 5.0$, Br = 0.2, $P = 0.2$, variable Bi.

hoc theory for capillary flows with varying levels of temperature dependence of density are identical to the predictions of the constant-density theory and given by the $P = 0$ curves in Figure 13. As in plane Poiseuille flow, these two theories cannot model the lowered temperature and velocity in the center of the conduit due to expansion cooling, and overpredict temperature and velocity for all values of the Biot number Bi. Likewise, as shown in Figure 17, the *ad hoc* theory (and equivalently the constant-density theory) overpredicts the volume flow rate at any given wall shear stress and heat-loss coefficient, and underestimates the values of wall stress beyond which no stable flow exists. Figure 17 also shows that the volume flow rate vs. wall shear stress curve predicted by the constrained theory for a given value of heat-loss coefficient h approximates the curve given by the ad hoc theory at a higher value of h. Thus, the temperature dependence of density in capillary flow produces roughly the same effect for volume flow rates as an increased heat-loss coefficient.

Flows in Annular Dies

We now model fully developed torsionless flows between two coaxial cylinders (Figure 18), as encountered in film-blowing and coextrusion processes. We define the shape parameter

$$m = \frac{r_1}{r_2 - r_1}, \tag{43}$$

where r_1 is the radius of the inner wall and r_2 the radius of the outer wall of the annular die. For fully developed torsionless flow we have

$$v_z = v_z(r), \qquad v_r = v_\psi = 0, \qquad \theta = \theta(r). \tag{44}$$

Our modeling differs from that of the second section in that here we allow differing heat-loss coefficients at the two bounding walls. This is because, although the designer can control the conduction of heat away from the outer die wall, the inner wall, being isolated by the moving fluid, must often be modeled as adiabatic or nearly adiabatic. The boundary conditions we adopt are therefore no slip at both walls,

$$\mathbf{v} = \mathbf{0} \quad \text{at} \quad r = r_1, \qquad \mathbf{v} = \mathbf{0} \quad \text{at} \quad r = r_2, \tag{45}$$

and the thermal boundary conditions

$$-k\frac{\partial\theta}{\partial r} = h_1(\theta - \theta_{c_1}) \quad \text{at} \quad r = r_1,$$

$$-k\frac{\partial\theta}{\partial r} = h_2(\theta - \theta_c) \quad \text{at} \quad r = r_2, \tag{46}$$

where in the most physically relevant case h_1 is zero (in which

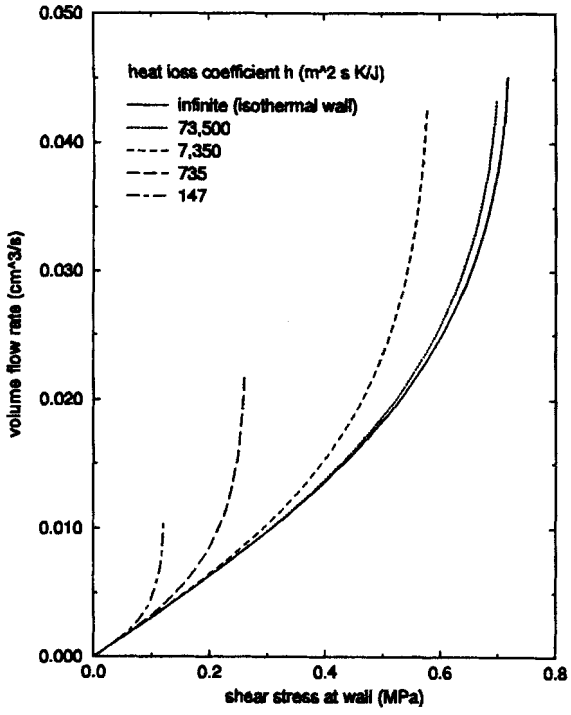

Figure 16. Effect of the heat-loss condition at the die wall on the relation between volume flow rate and wall shear stress for the PET melt flows of Table 2.

Predictions of the constrained theory.

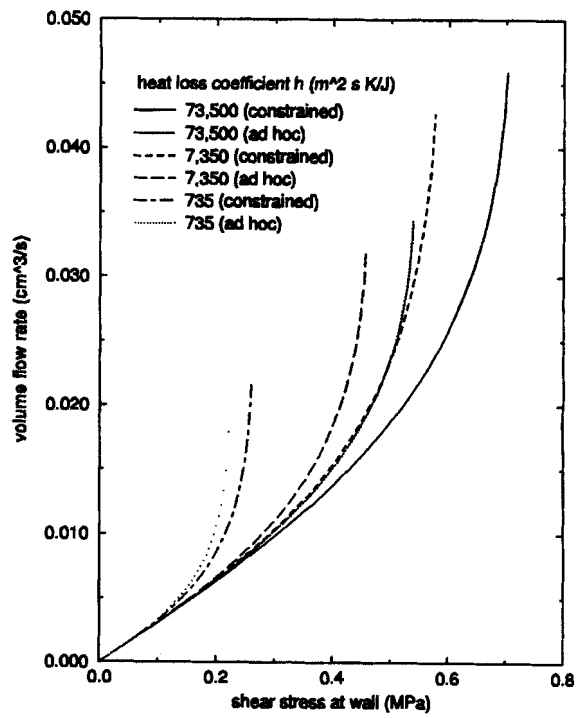

Figure 17. Volume flow rate vs. wall shear stress for the PET melt capillary flows of Table 2.

Comparison of the predictions of the constrained and *ad hoc* theories.

case the inner die wall temperature θ_{c_1} is irrelevant) or near zero.

Constrained theory

The dimensionless boundary-value problem for the fully developed annular flow of Figure 18 as modeled by the thermomechanically constrained theory, Eqs. 1–3, reduces to

$$\frac{d^2\tilde{v}_z}{d\tilde{\psi}^2}+\left(\frac{1}{\tilde{\psi}+m+\frac{1}{2}}-\frac{E}{\tilde{\theta}^2}\frac{d\tilde{\theta}}{d\tilde{\psi}}\right)\frac{d\tilde{v}_z}{d\tilde{\psi}} = -8\left(\tilde{\psi}+m+\frac{1}{2}\right)\exp\left[-E\left(\frac{1}{\tilde{\theta}}-1\right)\right], \quad (47)$$

Table 2. PET Flow Conditions Used in the Capillary Flow Simulations, and Corresponding Dimensionless Numbers

Flow conditions		
Capillary radius r_0	0.2	mm
Die temperature θ_c	285	°C = 558.2 K
Viscosity μ_c at die temp.	204.6	Pa·s
Shear stress at wall τ_w	Variable	
Heat-loss coefficient h	Variable	
Dimensionless numbers		
Arrhenius number E	12.18	
Brinkman number $\mathrm{Br}=\mathrm{Br}(\tau_w)$	$2.383\tau_w^2$	MPa^{-2}
Expansion number P	0.1869	
Biot number $\mathrm{Bi}=\mathrm{Bi}(h)$	$0.001361h$	$\mathrm{J\cdot m^{-2}\cdot s^{-1}\cdot K^{-1}}$

$$\frac{d^2\tilde{\theta}}{d\tilde{\psi}^2}+\frac{1}{\tilde{\psi}+m+\frac{1}{2}}\frac{d\tilde{\theta}}{d\tilde{\psi}} = -\mathrm{Br}\left(\frac{d\tilde{v}_z}{d\tilde{\psi}}\right)^2\exp\left[E\left(\frac{1}{\tilde{\theta}}-1\right)\right]+8\mathrm{Br}P\frac{\tilde{v}_z\tilde{\theta}}{1-P\tilde{\theta}}, \quad (48)$$

subject to the no-slip and heat-loss conditions at the walls,

$$\tilde{v}_z=0, \quad \frac{d\tilde{\theta}}{d\tilde{\psi}}=\mathrm{Bi}_1(a-\tilde{\theta}) \quad \text{at} \quad \tilde{\psi}=-\frac{1}{2},$$

$$\tilde{v}_z=0, \quad \frac{d\tilde{\theta}}{d\tilde{\psi}}=\mathrm{Bi}_2(1-\tilde{\theta}) \quad \text{at} \quad \tilde{\psi}=\frac{1}{2}. \quad (49)$$

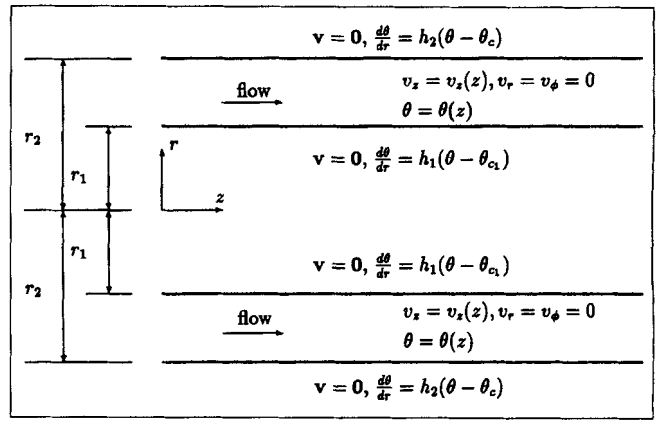

Figure 18. Fully developed annular flow.

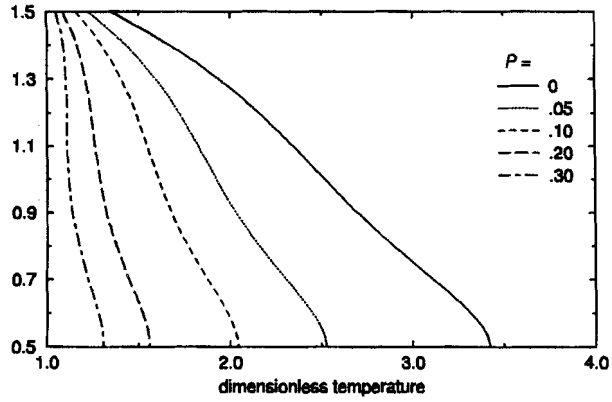

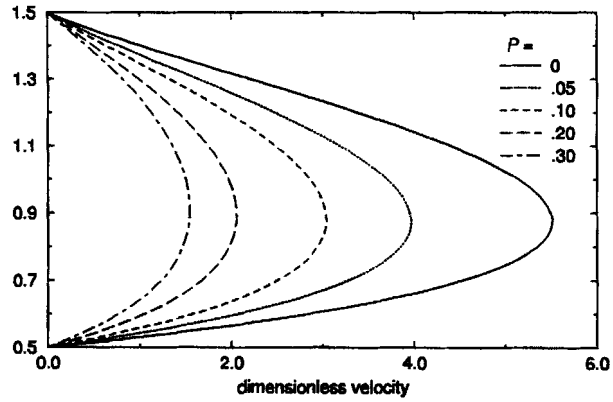

Figure 19. Velocity and temperature distributions in nonisothermal annular flows between an adiabatic inner wall and an outer wall with finite heat-loss coefficient, varying the level of temperature dependence of density.

$E = 3.0$, Br = 0.2, $Bi_1 = 0$, $Bi_2 = 10.0$, variable P; inner radius vs. wall separation $m = 0.5$. The vertical coordinate is the dimensionless transverse coordinate $\tilde{r} = r/(r_2 - r_1)$, with $\tilde{r} = 0.5$ the inner wall and $\tilde{r} = 1.5$ the outer wall.

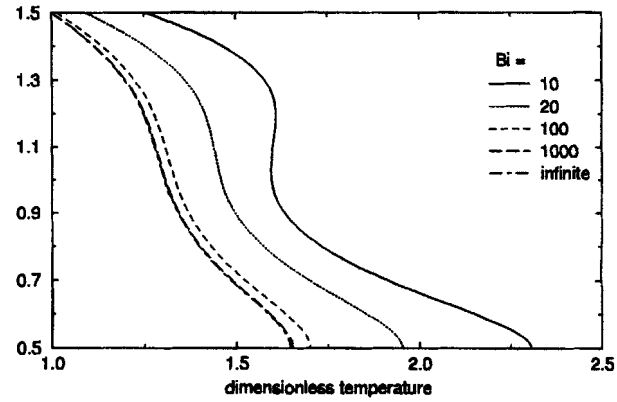

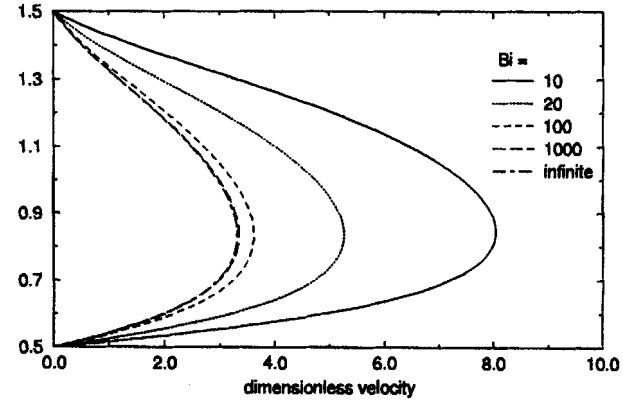

Figure 20. Velocity and temperature distributions in nonisothermal annular flows between an adiabatic inner wall and an outer wall with finite heat-loss coefficient, varying the heat-loss boundary condition.

$E = 5.0$, Br = 0.2, $Bi_1 = 0$, $P = 0.2$, $m = 0.5$, variable Bi_2.

In Eqs. 47–49,

$$\tilde{\psi} = \frac{r}{r_2 - r_1} - m - \frac{1}{2}, \qquad \tilde{\theta} = \frac{\theta}{\theta_c}, \qquad \tilde{v}_z = \frac{8\mu_c v_z}{\beta(r_2 - r_1)^2}, \tag{50}$$

and

$$\mathrm{Br} = \frac{\beta^2(r_2 - r_1)^4}{64k\mu_c\theta_c}, \qquad E = \frac{\varepsilon}{R\theta_c}, \qquad P = \frac{\rho_1\theta_c}{\rho_0}, \tag{51}$$

$$\mathrm{Bi}_1 = \frac{h_1(r_2 - r_1)}{k}, \qquad \mathrm{Bi}_2 = \frac{h_2(r_2 - r_1)}{k}, \qquad a = \frac{\theta_{c_1}}{\theta_c}. \tag{52}$$

The inner wall should usually be modeled with a small Biot number Bi_1.

Ad hoc and constant-density theories

If the annular flow of Figure 18 is modeled with the *ad hoc* theory, Eqs. 4–6, in which a temperature-dependent density function is substituted *a posteriori* in the incompressible equations, the dimensionless problem reduces to

$$\frac{d^2\tilde{v}_z}{d\tilde{\psi}^2} + \left(\frac{1}{\tilde{\psi} + m + \frac{1}{2}} - \frac{E}{\tilde{\theta}^2}\frac{d\tilde{\theta}}{d\tilde{\psi}}\right)\frac{d\tilde{v}_z}{d\tilde{\psi}} = -8\left(\tilde{\psi} + m + \frac{1}{2}\right)\exp\left[-E\left(\frac{1}{\tilde{\theta}} - 1\right)\right], \tag{53}$$

$$\frac{d^2\tilde{\theta}}{d\tilde{\psi}^2} + \frac{1}{\tilde{\psi} + m + \frac{1}{2}}\frac{d\tilde{\theta}}{d\tilde{\psi}} = -\mathrm{Br}\left(\frac{d\tilde{v}_z}{d\tilde{\psi}}\right)^2 \exp\left[E\left(\frac{1}{\tilde{\theta}} - 1\right)\right], \tag{54}$$

subject to the boundary conditions, Eq. 49. Again, as in the *ad hoc* theory's modeling of plane and capillary flows, temperature dependence of density has no effect on velocity and temperature, since P is absent from Eqs. 53 and 54. Note, however, that the annular geometry has coupled temperature to velocity in Eq. 54.

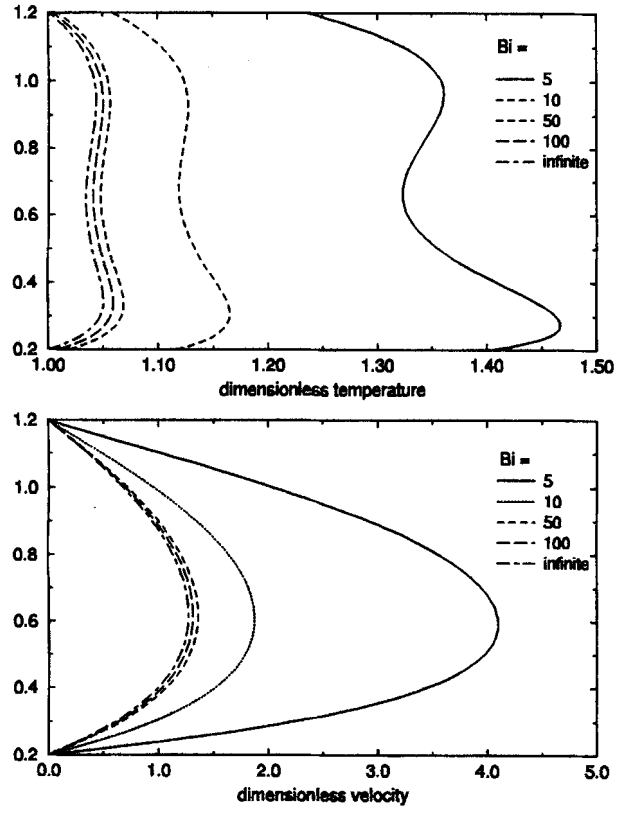

Figure 21. Velocity and temperature distributions in nonisothermal annular flows between inner and outer walls with the same heat-loss coefficient, for small shape parameter *m*.

$E = 5.0$, Br = 0.2, $P = 0.2$, $m = 0.2$, variable $Bi_1 = Bi_2 = Bi$.

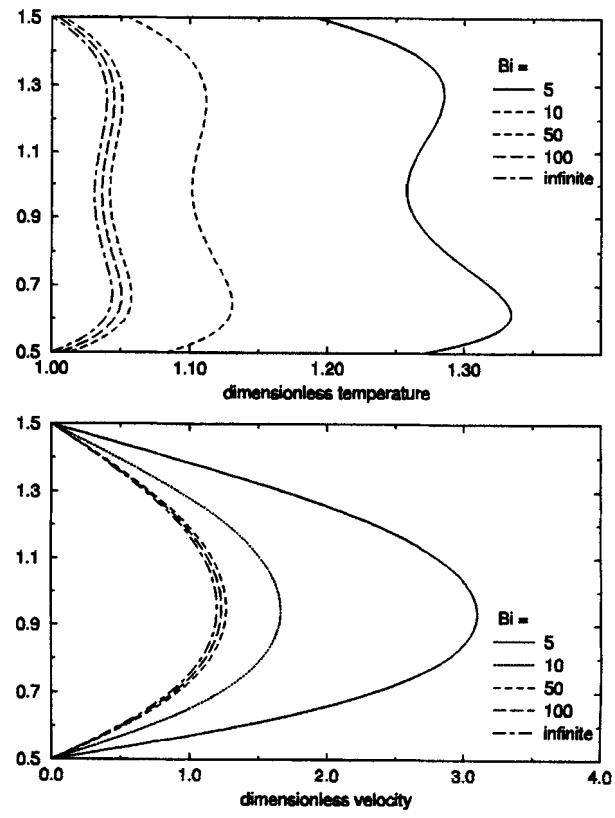

Figure 22. Velocity and temperature distributions in nonisothermal annular flows between inner and outer walls with the same heat-loss coefficient, for intermediate shape parameter *m*.

$E = 5.0$, Br = 0.2, $P = 0.2$, $m = 0.5$, variable $Bi_1 = Bi_2 = Bi$.

Predictions of the constrained theory

The effect of temperature-dependent density on velocity and temperature in the annular flows with an adiabatic inner wall and outer wall with finite heat-loss coefficient is shown in Figure 19. The prominent feature is the asymmetry between the inner and outer walls produced by the annular geometry and the differing thermal boundary conditions at the two walls. The fully developed flows exist for the adiabatic inner wall ($Bi_1 = 0$) because of the nonzero Bi_2 at the outer wall. If both walls are adiabatic, fully developed flows are not possible. The effect on velocity and temperature of varying the thermal boundary condition at outer wall while keeping the inner wall adiabatic is shown in Figure 20.

Figures 21–23 isolate the asymmetry to that due only to the annular geometry, by setting $Bi_1 = Bi_2$. We observe that the asymmetry of the temperature and velocity profiles becomes more pronounced with smaller ratio m, and, in the other direction, when the inner radius is more than twice the wall separation the profiles approach those for plane Poiseuille flow.

Conclusion

In this article we have employed the theory of Cao et al. (1995), which provides a simpler formulation than the unconstrained compressible theory yet retains essential temperature dependence of density, to model flows in slit, capillary, and annular dies with heat loss through the die walls. Heat loss is characterized by the Biot number, a combination of the wall heat-loss coefficient, fluid thermal conductivity, and wall separation, with the two limits $Bi \to \infty$ (isothermal walls) and $Bi = 0$ (adiabatic walls). We show that the expansion cooling phenomenon of depressed temperature in the center of the channel due to the competing effects of viscous heating and thermal expansion becomes more pronounced as Bi decreases from the isothermal wall limit. The depression in temperature occupies more of the channel in capillary dies than in slit and annular dies, with velocity significantly less sensitive to the thermal expansivity of the fluid. A feature discovered in this article is the possibility of multiple solutions in a small region of Biot number, thermal expansion number parameter space. (This feature was not discovered in Cao et al. (1995) since that article considered only isothermal walls ($Bi \to \infty$), and multiple solutions exist only for Bi between 6.3 and 20.1, and then only in a small range of P.)

We compared solutions of the thermomechanically constrained theory with solutions from both an *ad hoc* theory (based on the *a posteriori* substitution of temperature-dependent density into the governing equations for an incompressible material) and a constant-density model. We found that both the constant-density and *ad hoc* theories make quanti-

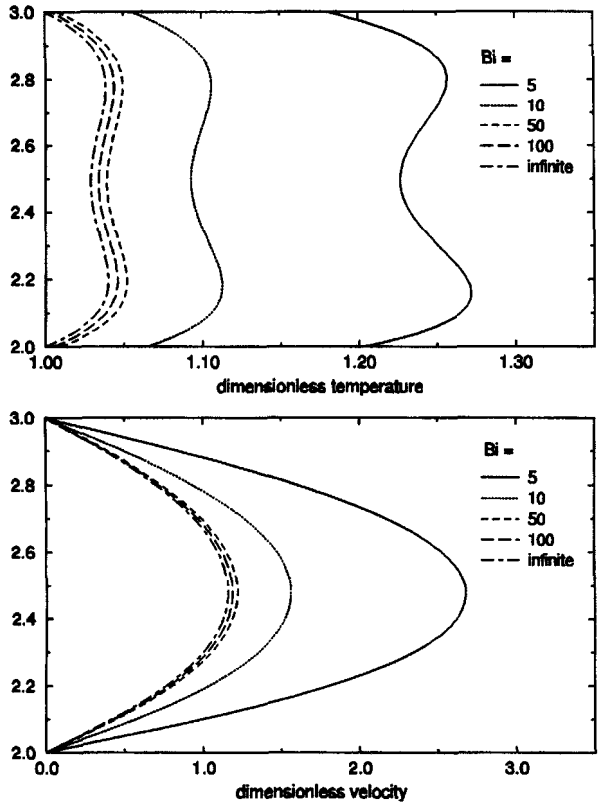

Figure 23. Velocity and temperature distributions in nonisothermal annular flows between inner and outer walls with the same heat-loss coefficient, for large shape parameter *m*.

$E = 5.0$, $\mathrm{Br} = 0.2$, $P = 0.2$, $m = 2.0$, variable $\mathrm{Bi}_1 = \mathrm{Bi}_2 = \mathrm{Bi}$.

tative and qualitative errors: neither theory can model expansion cooling, and both predict velocities and temperatures that are much too high. The errors magnify as $\mathrm{Bi} \to 0$, for example, for $\mathrm{Bi} = 1$ and $P > 0.1$ the *ad hoc* theory predicts temperatures so large as to abuse the assumption of linear dependence of density on temperature and return the nonsense of negative density. At any value of heat-transfer coefficient h the *ad hoc* theory overestimates the volume flow rate through the die at a given pressure gradient.

Acknowledgment

This research was funded in part by the Air Force Office of Scientific Research under grant F49620-93-1-0431 and the National Science Foundation under grant CTS-9319128.

Literature Cited

Brandrup, J., and E. H. Immergut, eds., *Polymer Handbook*, Wiley, New York (1989).

Cao, D., S. E. Bechtel and M. G. Forest, "The Constraint Response for a Material with Prescribed Temperature-dependent Density, and its Effects on a Fully-developed Nonisothermal Plane Poiseuille Flow," *J. Appl. Mech.*, in press (1996).

Cox, H. W., and C. W. Macosko, "Viscous Dissipation in Die Flows," *AIChE J.*, **20**(4), 785 (1974).

Duda, J. L., E. E. Klaus, and S. Lin, "Capillary Viscometry Study of Non-Newtonian Fluids: Influence of Viscous Heating," *Ind. Eng. Chem. Res.*, **27**, 352 (1988).

Dutta, A., "Role of Quench Air Profiles in Multifilament Melt Spinning of PET Fibers," *Text. Res. J.*, **57**, 13 (1987).

Hayashi, S., K. Tani, H. Ishihara, and H. Yasuda, "Fundamental Analysis of Hot Drawing in Spinline and Introduction of Basic Equations for Simulation," *Sen-I Gakkaishi*, **48**(10), 540 (1992).

Kase, S., and T. Matsuo, "Studies of Melt Spinning. I. Fundamental Equations on the Dynamics of Melt Spinning," *J. Poly. Sci.: Part A*, **3**, 2541 (1965).

Lodge, A. S., and Y. Ko, "Slit Die Viscometry at Shear Rates up to 5×10^6 s^{-1}: An Analytical Correction for Small Viscous Heating Errors," *Rheol. Acta*, **28**, 461 (1989).

Martin, B., "Some Analytical Solutions for Viscometric Flows of Power-Law Fluids with Heat Generation and Temperature Dependent Viscosity," *Int. J. Non-Linear Mech.*, **2**, 285 (1967).

Press, W. H., S. A. Teukolsky, W. T. Vetterling, and B. P. Flannery, *Numerical Recipes, The Art of Scientific Computing*, 2nd ed., Cambridge Univ. Press, New York (1992).

Spencer, R. S., and G. D. Gilmore, "Equation of State for High Polymers," *J. Appl. Phys.*, **21**, 523 (1950).

Sukanek, P. C., "Poiseuille Flow of a Power-law Fluid with Viscous Heating," *Chem. Eng. Sci.*, **26**, 1775 (1971).

Winter, H. H., "Viscous Dissipation in Shear Flows of Molten Polymers," *Adv. Heat Transfer*, **13**, 205 (1977).

Winter, H. H., "Temperature Fields in Extruder Dies with Circular, Annular, or Slit Cross-Section," *Poly. Eng. Sci.*, **15**(2), 84 (1975).

Manuscript received Sept. 25, 1995, and revision received Feb. 9, 1996.